Scattering and Absorption of Arbitrarily Oriented Dipoles with Finite Conductivity

H. Dominik
Institut für Hochfrequenztechnik
Technische Universität Braunschweig
P.O.Box 3329 , D-3300 Braunschweig
Federal Republic of Germany

Abstract

Plane wave scattering of lossy dipoles oriented arbitrarily in space is analyzed with the NEC-2 code. Modification of the code allows computing not only the radar cross section but also scattering and absorption cross section. With these electromagnetic characteristics it is possible to describe the relation between reradiated and absorbed power of the scatterer as a function of frequency and conductivity. A comparison with the results obtained with other codes (MININEC, Richmond) shows substantial differences at higher resonances of the dipoles.

1 Introduction

Electromagnetic scattering of randomly oriented wires has been investigated by many authors, mainly regarding application to chaff and scatter communication. Including finite conductivity yields an absorbing structure of lossy dipoles with maximal absorption at resonance frequency. Choosing a proper conductivity allows the design of absorbing chaff or resonance absorbers for EMI prevention consisting of lossy dipoles embedded in a suitable material.

In this paper the computed results of resonant dipoles with finite conductivity are analyzed for the broadside case with three different codes (NEC-2, MININEC, Richmond). In order to investigate the scattering of lossy dipoles it is necessary to compute not only the radar cross section but also the scattering and absorption cross section. Then it is possible to describe the relationship between reradiated and absorbed power and to optimize this ratio.

Assuming that all orientations of the dipoles are equally likely and averaging over all positions yields average cross sections.

2 Scattering and absorption cross section

Consider a wire with length $2l$ at broadside incidence of an electromagnetic wave with polarization parallel to the wire, as shown in Fig. 1. Divided into N segments the voltage across each segment is

$$V_n = \vec{E}_{\text{inc}} \; d_n \cdot \vec{u}_z \; , \tag{1}$$

with d_n the length of each segment and $\vec{E}_{\text{inc}}$ the electric field of the incident wave. The method of moments delivers the mutual impedances Z_{mn} between the segments. The solution of the matrix equation

$$[Z_{mn}][I_n] = [V_m] \tag{2}$$

yields the unknown currents I_n in the presence of the external field. If the wire is of finite conductivity κ, the self-impedances in the main diagonal of the impedance matrix are modified according to

$$\tilde{Z}_{mm} = Z_{mm} + R_m \; . \tag{3}$$

Taking the skin effect into account, R_m is a lumped load derived from the skin impedance per unit length [1]

$$Z_i = \frac{\mathrm{j}}{a}\sqrt{\frac{f\mu}{2\pi\kappa}}\left[\frac{\mathrm{Ber}(q) + \mathrm{j}\,\mathrm{Bei}(q)}{\mathrm{Ber}'(q) + \mathrm{j}\,\mathrm{Bei}'(q)}\right] \tag{4}$$

as

$$R_m = \Re e\{Z_i\}\; d_m \; , \tag{5}$$

with a the radius of the wire, f the frequency, μ the permeability of the wire material and $q = a\sqrt{2\pi f \mu \kappa}$ the argument of the Kelvin functions $\mathrm{Ber}(q)$, $\mathrm{Bei}(q)$ and their derivatives $\mathrm{Ber}'(q)$, $\mathrm{Bei}'(q)$, respectively. The total power input to the scatterer

$$P_{\text{i}} = \frac{1}{2}\sum_{n=1}^{N} \Re e\,\{V_n I_n^*\} \tag{6}$$

is split between losses dissipated in the lumped loads described by

$$P_{\text{d}} = \frac{1}{2}\sum_{n=1}^{N} R_n |I_n|^2 \tag{7}$$

and the power

$$P_s = P_i - P_d \tag{8}$$

scattered by the structure. With power density $S_{\mathrm{inc}} = \frac{1}{2}|\vec{E}_{\mathrm{inc}}|^2/Z_0$ ($Z_0 = 377\,\Omega$) of the wave incident on the structure one can define an absorption cross section σ_{A}, a scattering cross section σ_{S} and an extinction cross section σ_{E} according to

$$\begin{aligned} \sigma_{\mathrm{A}} &= P_{\mathrm{d}}/S_{\mathrm{inc}} \\ \sigma_{\mathrm{S}} &= P_{\mathrm{s}}/S_{\mathrm{inc}} \\ \sigma_{\mathrm{E}} &= P_{\mathrm{i}}/S_{\mathrm{inc}} \ . \end{aligned} \tag{9}$$

3 Differences between the used codes

The output file of NEC-2 delivers only the currents, but not the voltages across the segments in case of an incident plane wave [2]. Thus a WRITE-statement was included in the subroutine ETMNS, where the electric field at each segment is stored in a vector. With known lengths of the segments it is possible to compute the voltages across the segments and hence total input and absorbed powers.

MININEC allows only computations of antennas where one or more excitations are located at the connections between the segments [3]. To investigate scattering, one must first compute the induced voltages with (1) across the segments depending on the orientation of the segments to the incoming, known electric field $\vec{E}_{\mathrm{inc}}$. Exciting the wire with these voltages delivers the desired power with the computed currents. In order to by-pass the limit of 300 segments and to increase the computing precision, MININEC has been rewritten for FORTRAN using DOUBLE PRECISION data types.

The program of Richmond allows the computation of scattering and absorption cross section in case of an incident wave with no modifications required [4]. The disadvantage lies in the complicated input of each segment coordinate and all segment connections.

Beside the easy input the advantage of NEC-2 is the included computation of the frequency dependent loads with (4) and (5) for a given conductivity due to the skin effect, which normally must be taken into account . To allow an easy comparison between the different codes, the computed curves for absorption and scattering are obtained with a frequency independent resistance per segment. In general this is not a realistic model for the chosen geometry and swept-frequency computations, but the principal results are the same.

If in the following sections is no comment about the code being used, the curves are computed with NEC-2.

4 Scattering and absorption of a single dipole

The following computations are obtained for a dipole with parameters $2l$=0.482 m, a=0.123 mm and N=7. The radar cross section of a single lossless dipole is shown in Fig. 2a as a function of the normalized frequency $2l/\lambda$. Resonances occur if the length $2l$ is approximately an odd multiple of $\lambda/2$. Loading each segment with a constant resistance reduces the radar cross section σ at resonances according to Fig. 2b, but this is caused not only by absorption in the loads. As shown in Fig. 3 the current in a lossy dipole gets smaller, so σ is smaller due to a reduced backscattered electric field. For small values of conductivity the current nearly vanishes and the problem approaches backscattering by dielectric wires which is not considered here. So optimizing absorbing scatterers means to get little backscattered power while having large power dissipation.

The dependence of reradiated and absorbed power as function of the resistivity $\rho = 1/\kappa$ is shown in Fig. 4 near the first resonance. With increasing losses total power input decreases, and causes smaller currents. Absorption cross section will be equal to scattering cross section for one specific resistivity and greater for values larger than this resistivity. Choosing a value ρ greater than this resistivity, σ_A will be greater than σ_S only near the first resonance, as shown in Fig. 5. The ratio of absorbed to scattered power can be improved with lower conductivity, but only at expense of absorbed power. Thus sufficient absorption is only possible at first resonance.

As mentioned in the previous chapter due to the skin effect the variation of frequency yields different results for the cross sections depending on choosing a constant resistance or constant conductivity. Assuming a constant conductivity of $5.0 \cdot 10^4\,(\Omega\mathrm{m})^{-1}$ ($30\,\Omega$ at $2l/\lambda \approx 0.5$) yields a resistance of about 29 Ω at low values of $2l/\lambda$ and 41 Ω at $2l/\lambda$=3.0. The computed differences for Fig. 2 and Fig. 5 with this constant conductivity are so small that the assumption of a frequency independent resistance is justified for the considered frequency range.

To investigate the quality of lossy dipoles as absorbers, the dipole from Fig. 1 is arranged in front of an ideally conducting patch with area $A = 0.1\mathrm{m}^2$ lying in the x-z-plane, having the distance Δ from the patch. The radar cross section of this configuration as a function of Δ is shown in Fig. 6. Acting as a director the lossless dipole increases the radar cross section $\sigma/\lambda^2 = -9\,\mathrm{dB}$ of the single plate at 300 MHz for all distances. Losses lead to a significant reduction of σ if Δ is near multiples of $\lambda/4$. The first resonance occurs at a lower distance due to the large coupling between dipole and patch. The second and following resonances however indicate that this configuration acts as a kind of Salisbury screen absorber. The absorbing effects get smaller for larger patches, but this can be improved by a great number of dipoles.

Fig. 7 shows differences in the computed results between the three codes used, where the percental deviation from results computed with NEC-2 as function of the loads is shown. The deviations are very small, because according to (3) only the main diagonal elements of the impedance matrix are altered by adding the increasing values of the loads, and the currents following from the matrix system (2) with constant right side yield with (6) and (9) the extinction cross section.

In contrast to this the deviations in Figs. 8 and 9, showing the differences as function of frequency, are larger. To explain this behavior one must compute the currents induced on the dipole. For the current amplitude of a $\lambda/2$-dipole follows a half cosine as in Fig. 3, and the phase is nearly constant. Increasing the frequency produces current amplitude distributions with more and more cosine

periods. Looking at the phases shows that nearly constant phases only occur for $2l = 0.5\lambda, \lambda, 2\lambda, 3\lambda$. For $2l = 1.5\lambda$ and $2l = 2.5\lambda$ the phases of the currents differ from this smooth distribution including changes in the phase sign. The approximation of such complicated current distributions with the different codes leads to errors due to the basis functions used on the segments. The absorption cross section is computed with (7) and (9) and proportional to $|I|^2$. Because these deviations are smaller than those for the extinction cross section, which follows from I^* with (6) and (9), one can assume that the incorrect computation of the phases is responsible for the different results.

5 Average cross section of an arbitrarily oriented, single dipole

For arrangements of arbitrarily oriented wires it is important to know the average radar cross section of a single dipole. Then it is easy to estimate the average backscattering cross section, if the distance between the dipoles is greater than about 2 λ [5]. Smaller spacing will change the currents due to the coupling between dipoles. In this case it is mandatory to compute the currents of all dipoles depending on their distance and orientation to each other.

Assuming a constant polarisation of the incident wave as in Fig. 1 and averaging the backscattered field $\vec{E}_{\text{scat}}$ in the direction of the incident wave (monostatic case) over all possible positions of the dipole yields the average radar cross section $\bar{\sigma}$. Averaging the backscattered field $E_{\text{scat}} \cdot (-\vec{u}_z)$ with same polarisation as $\vec{E}_{\text{inc}}$ defines the average radar cross section for vertical polarisation $\bar{\sigma}_{\text{VER}}$, averaging over the backscattered field $E_{\text{scat}} \cdot \vec{u}_x$ perpendicular to $\vec{E}_{\text{inc}}$ leads to the average radar cross section for horizontal polarisation $\bar{\sigma}_{\text{HOR}}$.

σ_A and σ_S vary depending on the orientation of the dipole to $\vec{E}_{\text{inc}}$. Averaging over all dipole-positions for constant polarisation of the incident wave leads to average absorption and scattering cross sections $\bar{\sigma}_A$ and $\bar{\sigma}_S$.

If Θ- and Φ-orientations of the dipole are stepped linearly, Fig. 10 shows the configuration of all computed dipole positions when looking from the direction of the incident wave. The computed average radar cross sections for a lossless dipole $\bar{\sigma}_{\text{VER}}$ and $\bar{\sigma}_{\text{HOR}}$ are shown in Fig. 11. Additional peaks occur at even multiples of $\lambda/2$ due to non-broadside scattering. The computations agree very well with the results published in [6] except for the first resonance, where my cross section is higher. This may be caused by the restrictions used in [6], needed to develop a formula for the integral equation which can then be solved analytically.

Varying the positions randomly as suggested in [1] yields a similar pattern as in Fig. 10. Principal behavior of computed radar cross section is the same as in Fig. 11, but the curves have ripples near the minima, and the maxima are too high when using the same number of dipoles as for uniform distribution. Improvement is only possible for a great number of orientations.

Fig. 12 shows the average radar cross sections of lossy dipoles. The reduction of $\bar{\sigma}$ for all resonances is evident, but the behavior is the same as for the single dipole in section 4. Only near the first resonance the absorbed power is greater than the scattered as shown in Fig. 13, which shows the average absorption and scattering cross sections. The absorbing bandwidth increases with greater losses, but at cost of absolute power.

6 Conclusion

It is shown that a reduction of radar cross section of lossy dipoles is possible only near the first resonance and depends not only on absorbed power in the loads but also on decreasing currents producing a smaller backscattered electric field. With increasing losses the absorbed power is greater than the backscattered power near the first resonance. By choosing a small conductivity the absorbing bandwith can be improved, but only at cost of absorbed power.

Essential differences between the results of the three codes occur only for the lengths 1.5λ and 2.5λ of the dipole and can be interpreted as errors due to an incorrect computation of the current phase.

Allowing all directions for the dipole yields average cross sections. The scattering and absorption behavior is the same as for a single dipole at broadside incidence except for the radar cross section, where additional peaks occur according to non-broadside scattering.

References

[1] C.L. Mack,Jr., B. Reiffen: "RF chararcteristics of thin dipoles", Proc. of IEEE, Vol. 52, No. 5, May 1964, pp. 533-542

[2] G.J. Burke, A.J. Poggio: "Numerical Electromagnetics Code (NEC) – Method of Moments", NOSC Technical Document 116, Vol. 1, Lawrence Livermore Laboratory, Livermore, CA, Jan. 1981

[3] S.T.Li, J.W. Rockway, J.C.Logan, D.W.S.Tam: "Microcomputer tools for communications engineering", Artech House Inc., Washington ST., Dedham, MA, 1983

[4] J.H. Richmond: "Computer program for thin wire structures in a homogeneous conducting medium", Ohio State Univ., Jun. 1974, NASA-CR-2399

[5] R.G. Wickliff, R.J. Garbacz: "The average backscattering cross section of clouds of randomized resonant dipoles", IEEE Trans. Antennas and Propagation, Vol. AP-22, No. 3, May 1974, pp. 503-505

[6] J.H. Van Vleck, F. Bloch, M. Hamermesh: "Theory of radar reflection from wires or thin metallic strips", Journal of Applied Physics, Vol. 18, March 1947, pp. 274-294

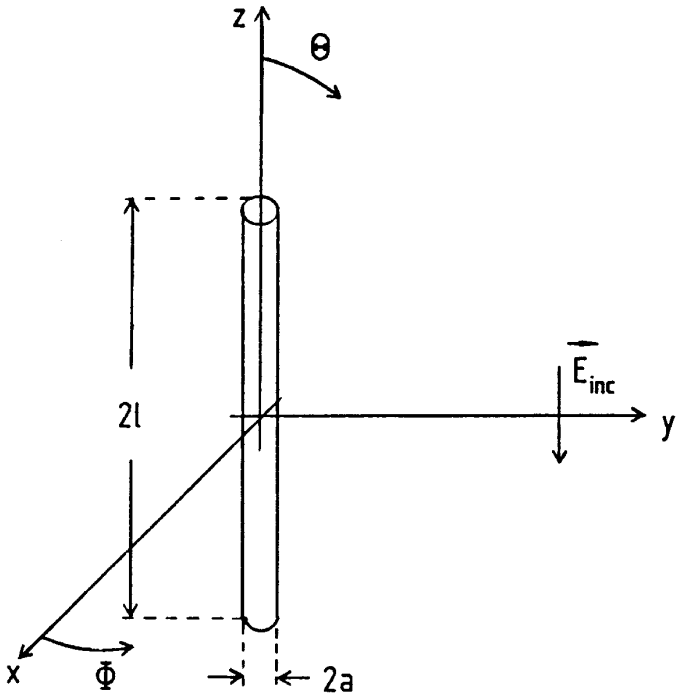

Figure 1: Dipole with length $2l$ and diameter 2a at broadside incidence of electromagnetic wave polarized parallel to the dipole

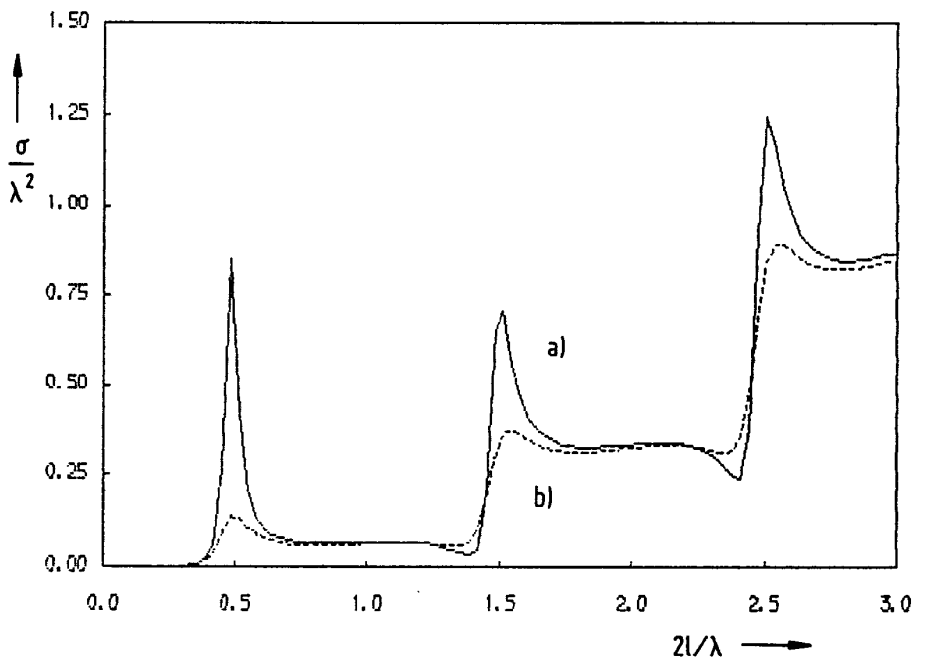

Figure 2: Normalized radar cross section σ/λ^2 as function of normalized frequency for a single dipole (N=7)
a) no losses b) each segment loaded with R=30 Ω

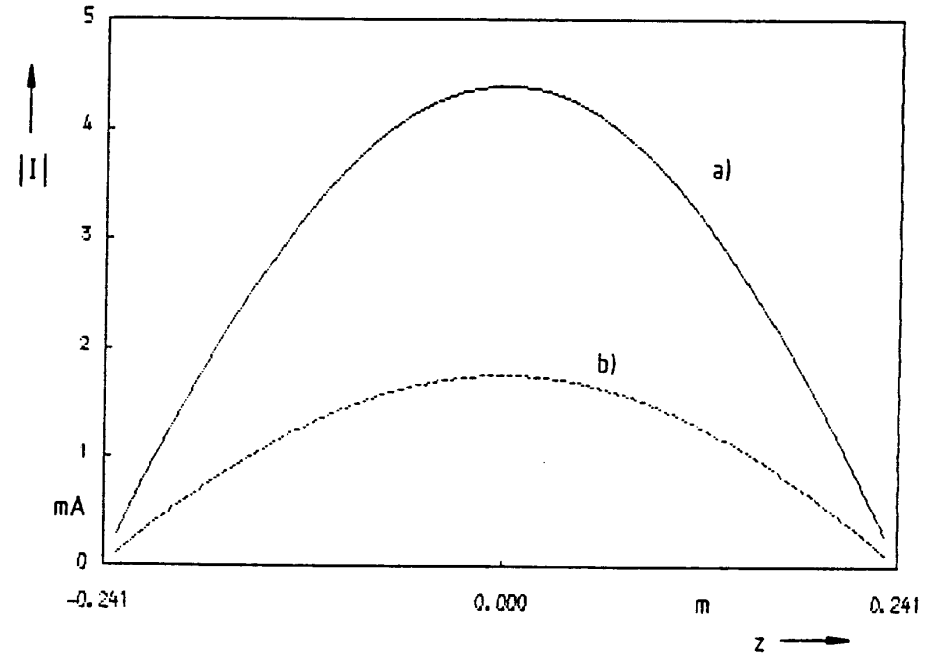

Figure 3: Current amplitude $|I|$ on a dipole for broadside case ($2l/\lambda \approx 0.5$, N=7)
a) no losses b) each segment loaded with R=30 Ω

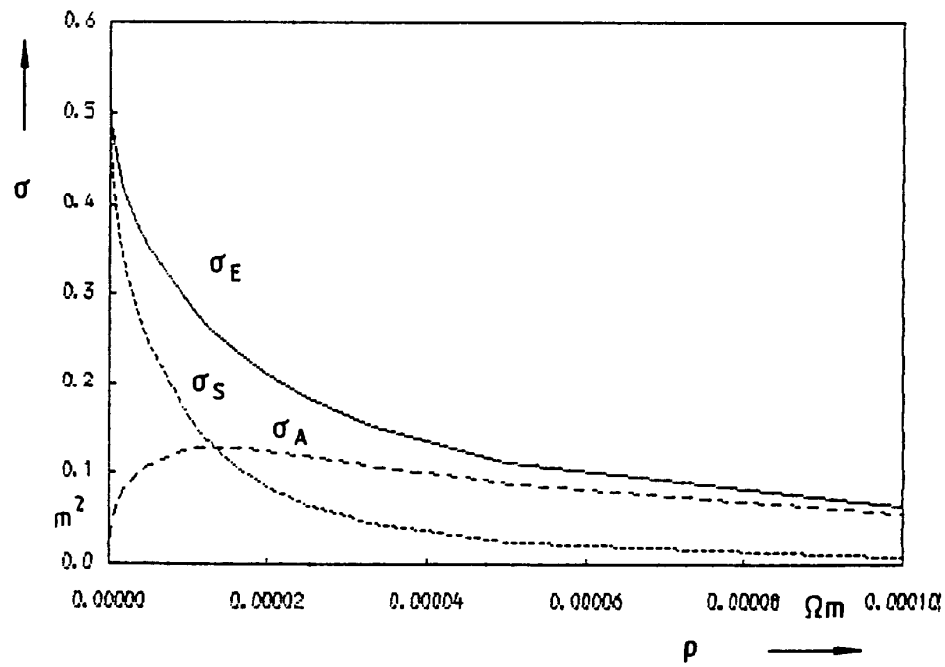

Figure 4: Extinction cross section σ_E, scattering cross section σ_S and absorption cross section σ_A as function of the resistivity ρ for a single dipole ($2l/\lambda \approx 0.5$, N=7)

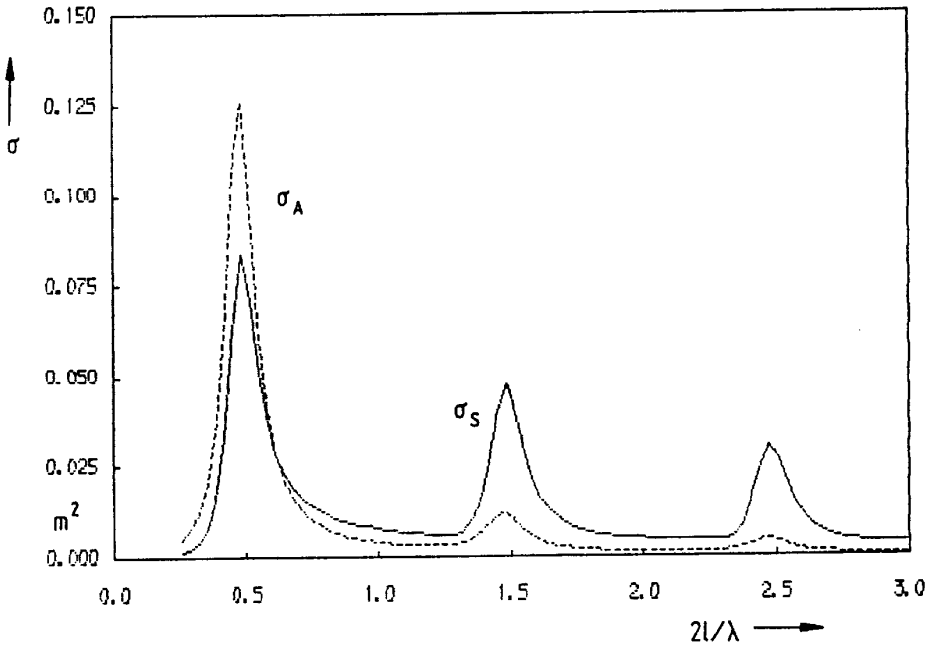

Figure 5: Scattering cross section σ_S and absorption cross section σ_A as function of frequency for a single dipole (R=30 Ω)

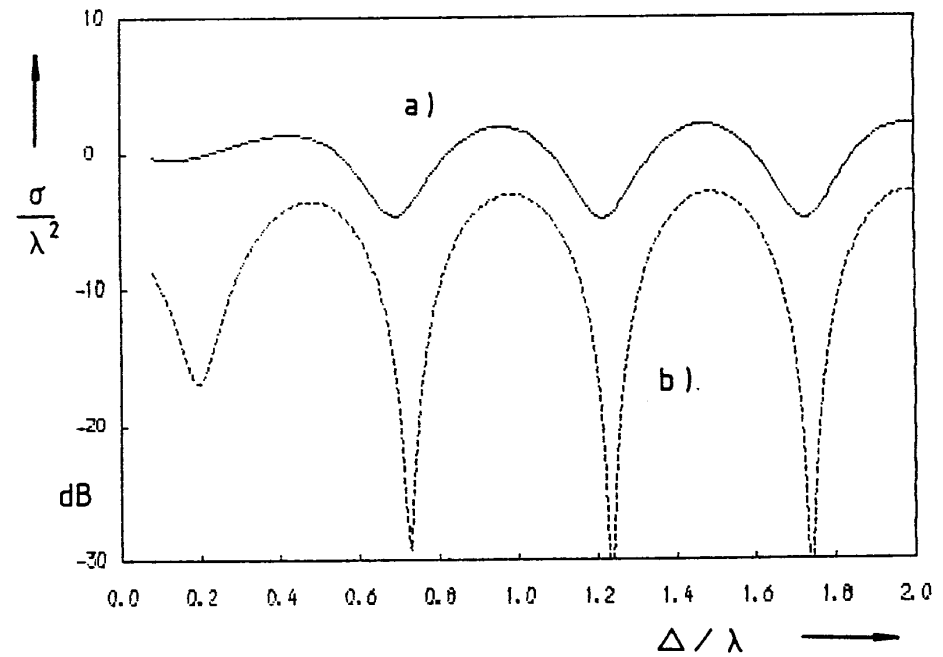

Figure 6: Radar cross section σ of a dipole in front of an ideally conducting patch with area $A = 0.1m^2$ as function of the distance Δ between patch and dipole ($2l/\lambda \approx 0.5$, N=7)
a) no losses b) each segment of dipole loaded with R=30 Ω

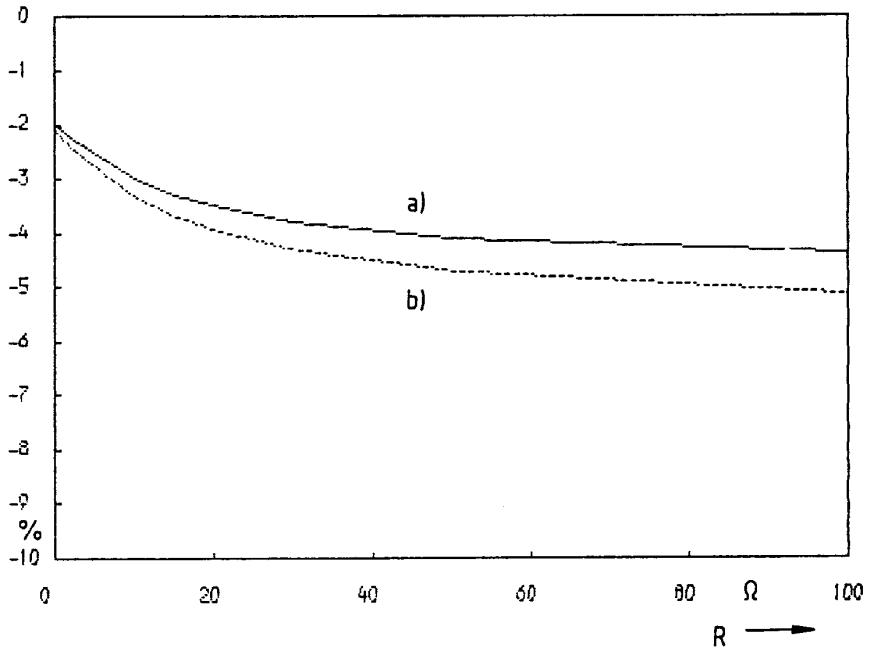

Figure 7: Percental deviation of extinction cross section from NEC as function of loads ($2l/\lambda \approx 0.5$, N=7)
a) Richmond b) MINI-NEC

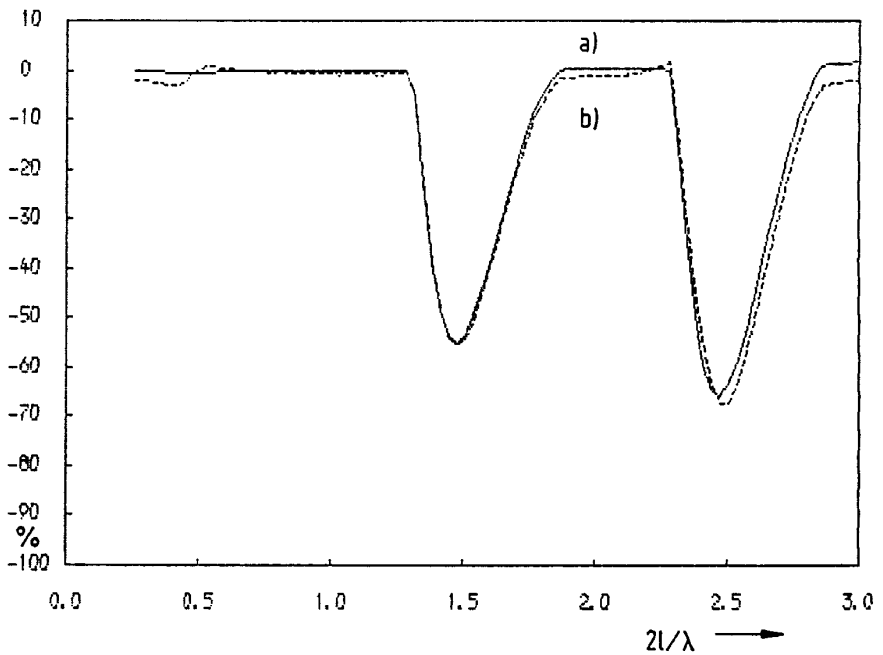

Figure 8: Percental deviation of extinction cross section from NEC as function of frequency (R=30 Ω , N=7)
a) Richmond b) MINI-NEC

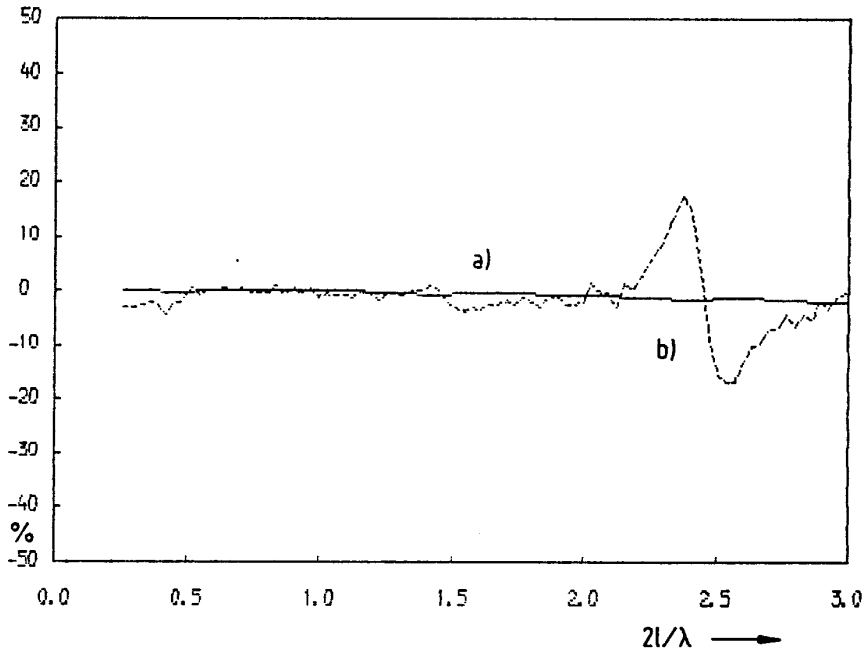

Figure 9: Percental deviation of absorption cross section from NEC as function of frequency (R=30 Ω , N=7)
a) Richmond b) MINI-NEC

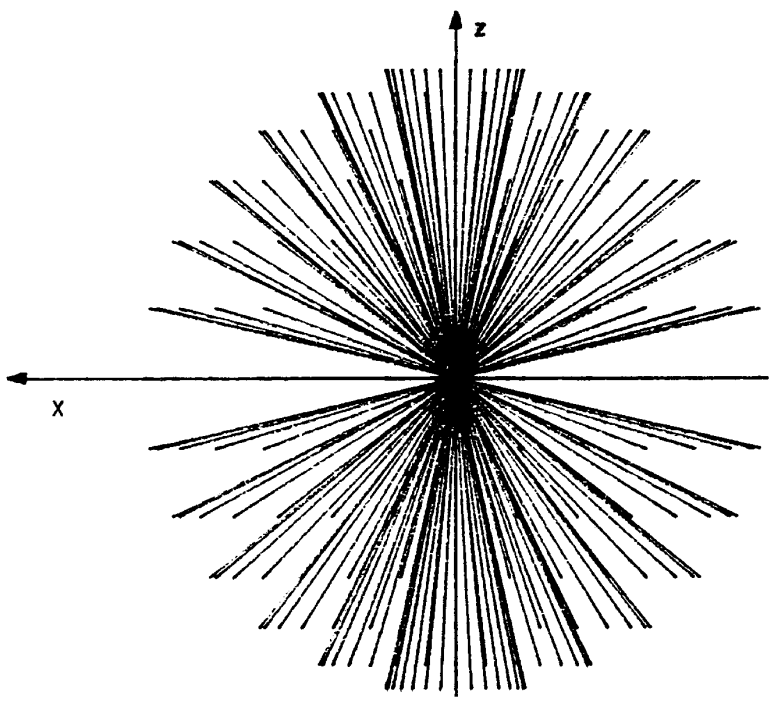

Figure 10: Stepping all possible dipole-orientations linearly in Θ− and Φ-direction yields the above configuration when looking from y-axis

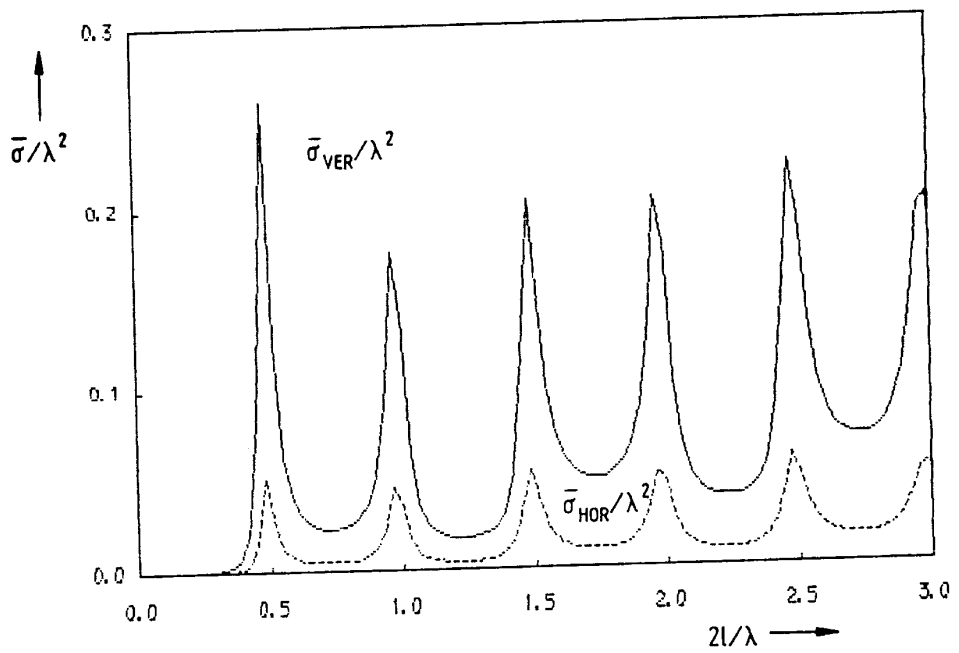

Figure 11: Average radar cross section $\bar{\sigma}_{VER}$ and $\bar{\sigma}_{HOR}$ as function of frequency for a dipole with infinite conductivity (N=7 , 183 orientations)

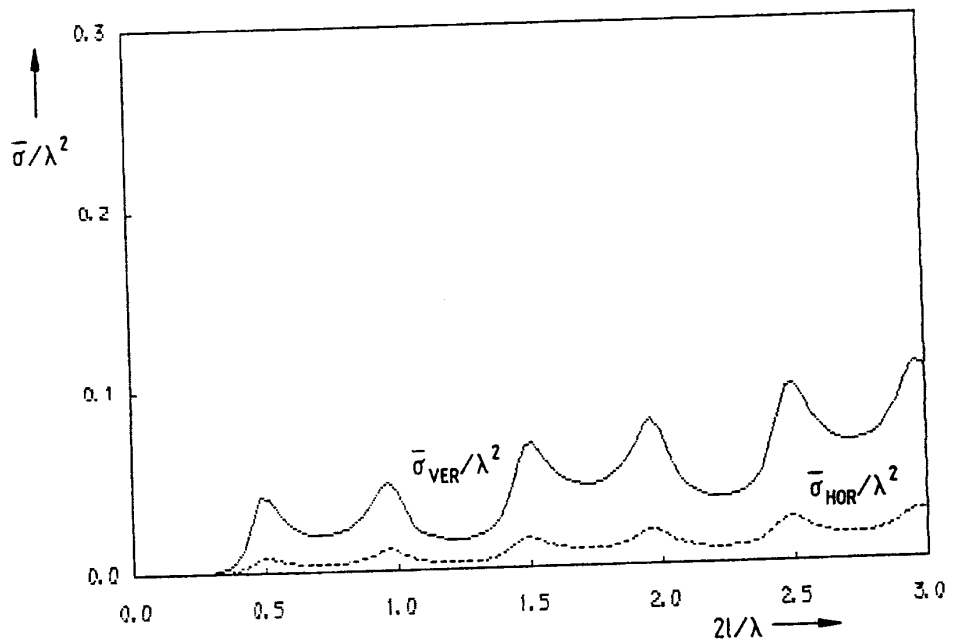

Figure 12: Average radar cross section $\bar{\sigma}_{VER}$ and $\bar{\sigma}_{HOR}$ as function of frequency for a dipole with lumped loads (R=30 Ω , N=7 , 183 orientations)

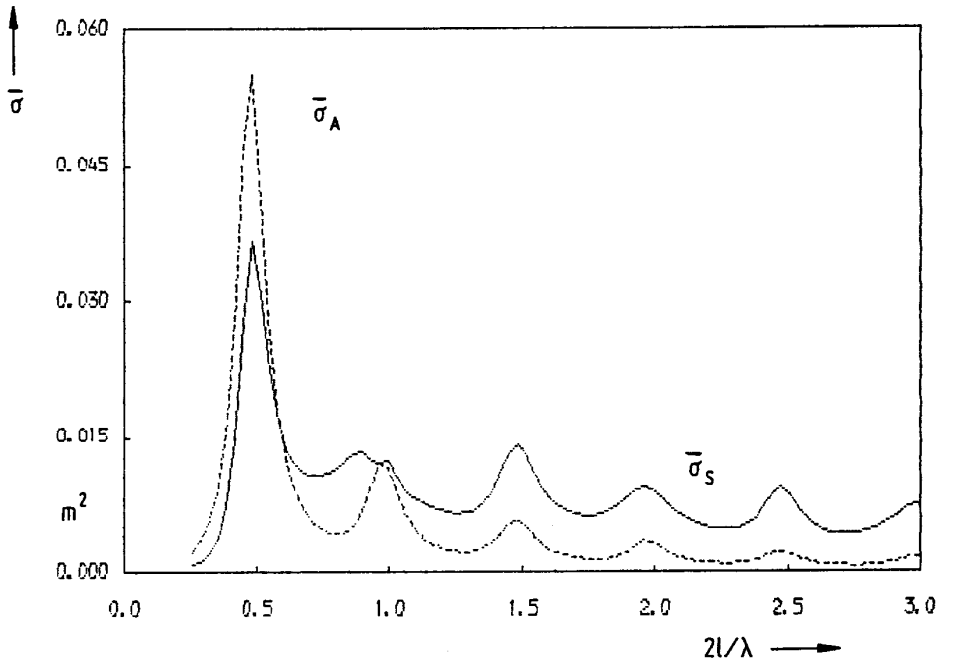

Figure 13: Average scattering cross section $\bar{\sigma}_S$ and absorption cross section $\bar{\sigma}_A$ as function of frequency for a dipole with lumped loads (R=30 Ω , N=7 , 183 orientations)